

Measurement of melting temperatures of some minerals under lower mantle pressures

Guoyin Shen¹ and Peter Lazor¹

Theoretical Geochemistry Program, Institute of Earth Sciences, Uppsala University, Uppsala, Sweden

Abstract. Melting temperature measurements of six minerals (stishovite (SiO_2), corundum (Al_2O_3), diopside ($\text{CaMgSi}_2\text{O}_6$), and three perovskites (MgSiO_3 , CaSiO_3 , $\text{Mg}_3\text{Al}_2\text{Si}_3\text{O}_{12}$)) at high pressures were carried out in a YAG laser-heated diamond anvil cell with rhenium metal as an absorber of the laser light. A polished or compressed disc of the sample was in contact with rhenium foil and heated by conduction. Melting was determined by plotting laser power/sample temperature function and looking for the thermal anomaly associated with the fusion of materials. All these solids were found to be highly refractory, requiring quite high temperatures for melting at the lower mantle pressures. The experimental melting results showed that for these minerals, melting temperatures increased with increasing pressure. Our results at low pressures are consistent with the data determined by other techniques (piston-cylinder, multianvils). The high-pressure melting of MgSiO_3 perovskite agreed with the recent measurements by Zerr and Boehler (1993) within experimental uncertainties. Melting temperatures and melting slopes of CaSiO_3 and $\text{Mg}_3\text{Al}_2\text{Si}_3\text{O}_{12}$ perovskites were found to be less than those of MgSiO_3 perovskite, indicating that the presence of Ca and Al would decrease the melting temperatures of MgSiO_3 perovskite in the Earth's lower mantle and that this effect will increase with increasing pressures. Melting temperature measurements on stishovite and corundum to pressures of 36 GPa and 25 GPa, respectively, are reported.

Introduction

The presence of a light crust with high concentrations of large-ion lithophile elements and a dense iron core indicates that the Earth is a differentiated body. It is generally accepted that the stratification of the Earth is a result of gravitational separation of materials according to their melting points and densities [e.g., Anderson, 1989]. Melting should therefore be considered as one of the most important processes affecting the evolution of the planet. In addition, data on melting temperatures are also significant for an understanding of the convection at depth, for example, viscosities of materials scale according to the ratio of temperature to the melting temperature [Weertman and Weertman, 1975]; the melting relations set constraints on the geothermal gradient of the Earth's interior [Boehler, 1993; Saxena et al., 1994]. Knowledge of high-pressure melting is thus of fundamental importance in understanding the chemical composition, convective movement, and thermal evolution of the Earth's interior.

High-pressure and high-temperature studies now indicate that the perovskite-structured silicates (e.g., $(\text{Mg,Fe})\text{SiO}_3$) plus magnesiowüstite ($(\text{Mg,Fe})\text{O}$) are the dominant phases in the lower mantle [Liu, 1976; Mao et al., 1977; Knittle and Jeanloz, 1987; Ito and Takahashi, 1989]. Melting curves of $(\text{Mg,Fe})\text{SiO}_3$ perovskite and wüstite have been determined to lower mantle pressures with the diamond anvil cell technique

[Heinz and Jeanloz, 1987; Knittle and Jeanloz, 1989; Boehler 1992; Shen et al., 1993; Sweeney and Heinz, 1993; Zerr and Boehler, 1993]. However, these data show large discrepancies both in melting temperatures and slopes of melting curves and yield extremely different estimations of the melting temperature in the lower mantle; for example, melting temperatures of $(\text{Mg,Fe})\text{SiO}_3$ -perovskite range from 2500 K to 8000 K at pressures equivalent to those at the bottom of the mantle. Melting data for MgSiO_3 perovskite with the multianvil technique have been obtained in the pressure range of 21–25 GPa [Ito and Katsura, 1992]. This pressure range spans only the uppermost part of the lower mantle and yields a weak constraint on the melting slope of perovskite. Thus more measurements are needed to have a consensus on melting at lower mantle pressures.

CaO and Al_2O_3 are likely to be the next most abundant components of the lower mantle. Melting relations in the lower mantle will be affected by the presence of Ca and Al. X ray investigations of high-pressure samples (50 GPa) of peridotite [O'Neil and Jeanloz, 1990] suggested that $(\text{Mg,Fe})\text{SiO}_3$ perovskite, CaSiO_3 perovskite and $(\text{Mg,Fe})\text{O}$ magnesiowüstite are stable at this pressure. Mao et al. [1989] found that CaSiO_3 perovskite is stable for all lower mantle pressures. Weng et al. [1982], on the basis of high-pressure measurements on the system MgSiO_3 - CaSiO_3 - Al_2O_3 , concluded that CaSiO_3 perovskite forms a separate phase. Mao et al. [1977], Tamai and Yagi [1988], and Irifune et al. [1989] found that diopside decomposes into mixtures of MgSiO_3 components and CaSiO_3 perovskite at pressures above about 18 GPa at 1000°C. In the system MgSiO_3 - Al_2O_3 , it was observed that a small amount of Al_2O_3 (at least 25 mol%) dissolves in MgSiO_3 perovskite at pressures above about 30 GPa [Liu, 1977; Weng et al., 1982; Irifune and Ringwood, 1987]. So it is likely that at high pressure and temperature,

¹Now at Geophysical Laboratory, Carnegie Institution of Washington, Washington, D.C.

CaSiO₃ perovskite exists as a separate phase, whereas Al₂O₃ dissolves in MgSiO₃ perovskite. Melting curves of CaSiO₃ perovskite and Mg₃Al₂Si₃O₁₂ perovskite at lower mantle conditions will provide constraints upon the Ca and Al effect on melting relations of the lower mantle rocks.

Although free SiO₂ and Al₂O₃ are unlikely to be present in substantial quantities in the lower mantle, they are constituents of lower mantle minerals. Melting data of stishovite (SiO₂) and corundum (Al₂O₃) will put an end-member constraint in modeling the melting relations in the system of FeO-CaO-Al₂O₃-MgO-SiO₂, which represents the lower mantle chemistry.

In this study, we examined the melting of MgSiO₃ at pressures up to 42 GPa using a YAG laser-heated diamond anvil cell. We also conducted melting experiments on diopside (CaMgSi₂O₆), pyrope (Mg₃Al₂Si₃O₁₂), wollastonite (CaSiO₃), stishovite (SiO₂), and corundum (Al₂O₃) to clarify the effects of calcium and aluminum on the melting of MgSiO₃ perovskite and to produce high pressure melting data of end member minerals.

Experimental Procedure

Starting Materials

Two types of samples were used. One was in a single-crystal form, the other was in powder form. For crystal samples (enstatite, diopside, wollastonite, and ruby), the crystal was polished to the thickness of about 10 μm. Powder samples (stishovite and pyrope) were loaded into a gasket chamber and compressed by diamond anvils until becoming transparent. The thickness of the powder disc was about 10-20 μm. Synthetic orthoenstatite in a single-crystal form was synthesized from a stoichiometric mixture of MgO and SiO₂ and was provided by H. Skogby. Natural diopside and wollastonite in single crystal form were from Zillerthal, Austria, and Perheniemi, Finland, respectively. The crystals showed a good quality under microscope. Microprobe analysis of diopside and wollastonite is shown in Table 1. Ruby was corundum crystal with 0.5 wt% of Cr₂O₃. Pyrope and stishovite samples were synthesized at Stony Brook and were provided by R. Liebermann and J. Zhang. Experimental procedures of pyrope and stishovite synthesis were described by Zhang and Herzberg [1994] and Zhang et al. [1993], respectively. X ray diffraction pattern showed a single phase for each samples.

High-Pressure and High-Temperature Technique

The laser-heated diamond anvil cell (DAC) technique was used. This technique has been widely adopted to study the

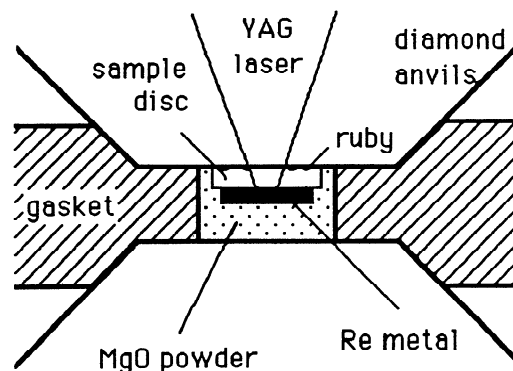


Figure 1. Schematic cross section of a diamond anvil cell assemblage.

high-pressure/temperature regime of the Earth's interior. The recent measurements on the phase transition and melting of a few geophysically important materials to extremely high pressures have provided constraints on the thermal states of the Earth's lower mantle and the core [e.g., Boehler, 1993; Saxena et al., 1993]. For metallic or opaque materials, such as iron, nickel, and wüstite, the samples absorb YAG or YLF laser light well, and melting can be identified by in situ visual observation and by checking discontinuities in collected signals, such as temperature and reflectivity, as a function of laser power [e.g., Boehler et al., 1990; Shen et al., 1993]. For mantle silicates, which do not absorb YAG or YLF laser light well, a CO₂ laser with high output power was used to heat the sample to sufficiently high temperatures [Boehler and Chopelas, 1992; Yagi and Susaki, 1992]; or by placing in contact with an opaque metal, the sample was heated by conduction from the metal [Heinz and Sweeney, 1992]. By the metal-contact method, a stable Nd:YAG laser can be used to heat a metal absorber with a high melting point, and melting temperatures can be determined by looking for the thermal anomaly associated with the melting of transparent samples. In this study the metal-contact method was used. Rhenium metal was chosen as a metal absorber because of its chemically inert property and high melting point (3453 K at 1 atm). Experiments were carried out in a continuous YAG laser-heated diamond anvil cell. The system was described in detail elsewhere [Lazor et al., 1993; Shen et al., 1993].

Cell Assembly

The high pressure cell geometry is shown in Figure 1. Standard designed type I diamonds with culet diameters of 0.45 mm were used. Stainless steel T301 gasket with 0.40-mm thickness was indented between diamond anvils, and a 200-μm diameter hole was drilled at the center of the indentation. The rhenium metal, a foil of ~10-μm thickness, was loaded into the hole over a layer of fine-grained MgO powder, which served as a pressure medium. For samples that would be run for X ray diffraction, SiO₂ gel in fine powder form was used as pressure medium. Rhenium metal was chosen because of its chemical stability and high melting point. The chemical reactivity of rhenium depends on the manner in which it is prepared [Clark, 1952]: the polished compact metal is much less reactive than the powder. In our preparation, rhenium was cut in a small piece, then flattened to about 10 μm in thickness by pressing between the diamond anvils. In this way, we got a compact metal foil with a quite smooth surface. A polished or compressed sample disc was put over, and in direct contact

Table 1. Microprobe Analysis of Diopside and Wollastonite

Oxide	Diopside, Wt.% ± s.d.	Wollastonite, Wt.% ± s.d.
Na ₂ O	0.026 ± 0.022	0.006 ± 0.012
MgO	17.207 ± 0.177	0.000 ± 0.000
Al ₂ O ₃	0.008 ± 0.011	0.001 ± 0.003
SiO ₂	54.703 ± 0.167	50.908 ± 0.072
K ₂ O	0.004 ± 0.007	0.002 ± 0.004
CaO	25.961 ± 0.227	48.920 ± 0.216
MnO	0.140 ± 0.039	0.005 ± 0.006
FeO	1.565 ± 0.137	0.086 ± 0.042
Total	99.614	99.939

with, the rhenium foil. Several small ruby chips were spread over the assemblage for pressure measurements. The whole assemblage was then dried at 105°C for at least 12 hours and was sealed later by two diamond anvils in vacuum condition. This drying procedure was important for eliminating any possible chemical reaction due to the presence of moisture.

For each experiment, four quantities were measured: pressure, temperature, incident YAG laser power, and the reflectivity of YAG laser light from the heating spot.

Pressure Measurement

Pressure was measured using the ruby-fluorescence technique [Mao *et al.*, 1978, 1986]. Pressure distribution across the sample was measured before and after heating. Uncertainties in pressure determination depend on the accuracy of the ruby scale, the pressure gradient across the sample, the magnitude of pressure drop after laser heating, and thermal pressure estimation. The ruby scale has an error of 6% over the pressure range of present study [Mao *et al.*, 1978]. Uncertainties due to the pressure gradient across the spot (10 μm) were found to be approximately ± 1 GPa at 10 GPa and ± 2.5 GPa at 50 GPa. The magnitude of the pressure decrease following laser heating was about 10-15% of the initial pressure. Usually, pressure dropped most after the first heating; further heating did not change the pressure much (1-3%). Therefore this error could be minimized by heating a chosen spot. The thermal pressure estimation was considered as a theoretical task. Heinz [1990] considered the thermal elastic effect on thermal pressure and calculated that the thermal pressure in the thermal elastic case is approximately one-half the expected thermodynamic thermal pressure. In this work it was assumed that the magnitude of thermal pressure is about 7% of the pressure after heating [Shen *et al.*, 1993]. It should be noted that the thermal pressure in a laser-heated diamond anvil cell is not well understood at present. Raw measured pressures before and after heating will be also presented. Random errors from pressure gradient and pressure drop after laser heating were estimated as 7-12%.

Temperature Measurement

Temperature of the laser-heated spot was measured using essentially the same spectroradiometric system as that described by Lazor *et al.* [1993]. Some technical improvements and modifications have been made since then: (1) A laser power controller (LPC, Cambridge Research & Instrumentation) [Heinz *et al.*, 1991] was introduced into the system and improved the power stability to variations of less than 0.5%, which resulted in high reproducibility in the temperature and reflectivity measurement. (2) A new sensitive charge-coupled device (CCD) detector (Oriel, Instaspec IV) allowed to measure temperature as low as 1000 K and hence a large range of power-temperature relation. (3) A wavelength range from 754 nm to 1065 nm was chosen so that reflection of YAG laser light ($\lambda = 1064$ nm) from the heating spot could be measured at the same time as the radiation emitting from the spot was collected. Temperatures were measured from the rhenium metal foil, which was in direct contact with samples. Temperatures were measured in situ from the center of a hot spot from areas with about 3 μm in diameter. The radiation spectra were fitted to Planck's radiation function in the range from 754 nm to 939 nm, solving for both temperature and absolute emissivity. Wavelength dependence of emissivity for

rhenium [Cabannes, 1967] was taken into account in fitting procedures, and it was assumed that the dependence still holds at high pressure and temperature.

There are several sources of uncertainty in temperature measurement: (1) inaccuracy of calibration function from a National Institute of Standards and Technology (NIST) calibrated halogen tungsten lamp, (2) aberration effect of optics, (3) nonlinearity of response of the detector, (4) inaccuracy of emissivity data at high pressure and temperature, (5) statistical errors in fitting to Planck's function, (6) power instability and point instability of YAG laser, and (7) temperature gradient across the heating spot. The first three were considered as systematic errors, which were proved to be not significant by measuring a series of materials with known melting temperatures [Saxena *et al.*, 1994]. At the present stage, it is difficult to consider the emissivity-wavelength function at high pressure from both theory and available data. Wavelength-independent emissivities were assumed by Heinz and Jeanloz [1987] and Boehler [1993]. For Re metal at 1 atm, the temperature correction by the emissivity-wavelength function [Cabannes, 1967] is about 100 K at 2500 K and about 180 K at 3500 K. In this study we employed the emissivity-wavelength function at 1 atm and assumed that the dependence remains the same at high pressure. Errors from this assumption would not exceed 200 K in the temperature range studied. The statistical errors due to fitting were found to be ± 5 at 2000 K and ± 20 at 3500 K; the temperature fluctuations from laser instability were found to be ± 15 K for the exposure time of 0.1 s at 2500 K. The radial gradient within the heated area depends on the YAG laser beam's degree of focus on samples. To have the lowest temperature gradient in the sample, the beam was usually defocused to a degree necessary for achieving the desired temperatures. For a temperature of 2085 K, the radial gradient was measured to be ~ 20 K/ μm in the center (3 μm in diameter) of the hot spot; for a temperature of 3150 K, it was ~ 60 K/ μm . From (5), (6), and (7), the total random error was estimated to be $\pm 50 - \pm 100$ K, depending on the temperature range. The error values were in accordance with melting point repeatability of Pt, Re, and W metals at 1 atm.

Reflectivity Measurement

Nd:YAG laser light has a wavelength of 1064 nm. A wavelength range from 754 nm to 1065 nm was chosen so that both the YAG laser reflection and thermal radiation from the heated spot were measured at the same time. Since the intensity of the reflected laser light was measured from the very same area as the thermal radiation at the same time, its measurement served as an independent method of characterizing the laser-heated area. Because of the laser's instability and changes in some physical properties (absorption, texture, etc.) during heating, the measured reflectivity against incident laser power usually does not show a smooth curve. Range 1 in Figure 2 shows that the reflectivity curve is not as smooth as the temperature curve. It appeared that the reflection signal was more sensitive to experimental conditions than the radiation signal. In Figure 2, a large change in reflectivity appeared along with the thermal anomaly in range 2. This was interpreted as the change in physical properties due to melting. Because of the sensitivity of the reflection signal, sometimes it was difficult to judge whether the change in intensity was due to the melting or some other factors. Therefore, the reflection signal was used as a secondary criterion for melting detection.

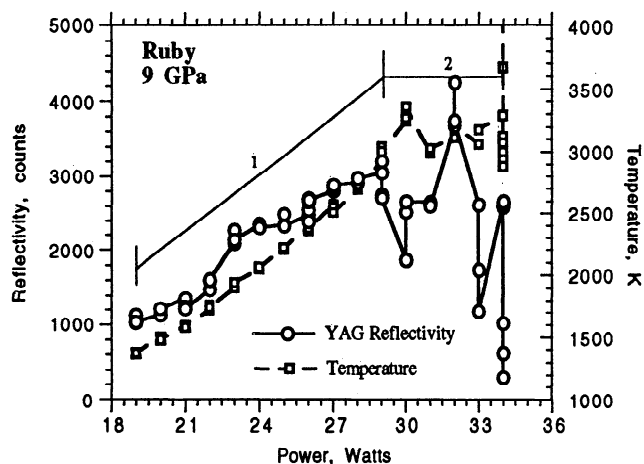


Figure 2. The measured YAG reflectivity and temperature as a function of laser power at 9 GPa for ruby. In range 1, sample temperature increases smoothly with increasing laser power, but reflectivity of YAG laser light from the heating spot shows fluctuation with power. The strong change in reflectivity appears along with the thermal anomaly in range 2. Because of the sensitivity of the reflection signal, sometimes it is difficult to judge whether the change in intensity is due to the melting of materials by the reflection signal alone. Therefore reflection signal is used as a secondary source of characterizing melting.

Nd:YAG Laser Power Measurement

It was possible to control and read laser power directly from the laser power controller. However, we found that the working range of the LPC was limited from 20 W to 32 W at the maximum input power of the YAG laser (35 W). To have a larger working range, a continuously variable attenuator was put at the output of the LPC in our laser heating system. By fixing a power output from the LPC (usually at 32 W), we were able to regulate power from 0 W to 30 W by rotating a $\lambda/2$ plate. Laser powers were measured through the secondary beam from the beam splitter cube. This method also avoided possible power instability arising from regulating the LPC. The obtained laser power was stable within ± 0.01 W.

Melting Characterization

Melting was determined by plotting the laser power/sample temperature function and looking for the thermal anomaly associated with melting. The melting temperature measured by the thermal anomaly was in agreement with the observed change in reflectivity of YAG laser light. The melting temperatures of diopside, enstatite, and pyrope determined at low pressures by this method were found to be consistent with the data from other techniques [e.g., Boyd and England, 1963; Irifune and Ohtani, 1986; Presnall and Gasparik, 1990]. The various starting materials give various, nonidentical results. This indirectly argues against the possibility that we are seeing some artifact of recrystallization or melting of Re metal. The various compositions also give values which are sensible and internally consistent with one another.

Temperatures were measured at least three times at each step as the laser power was increased. The time interval between two temperature measurements was about 30 s. The power step varied between 0.2 and 0.3 W. On melting, there was a sudden increase in temperature within a small power change.

Therefore, steps as small as 0.1 W were sometimes used to precisely determine the thermal anomaly. One experimental run usually lasted an hour.

Each run started with a low laser power to get a large range of power-temperature relation and, moreover, to let the sample convert completely to high-pressure phases at the heating spot. Figure 3 shows an example of experiments in which temperatures and YAG laser reflectivity were plotted as a function of the laser power at 9.4 GPa for diopside. The temperature increases smoothly with power, while the YAG laser reflectivity is not as smooth. When temperature reached around 2360 K, it started to fluctuate and there was no more increase in temperature within a few more steps of increasing power. There was also a big change in intensity of YAG reflectivity within this fluctuation range. This fluctuation in temperature was interpreted as the melting of diopside. The temperatures measured during the fluctuation were close to those of melting determined by the multianvil apparatus [Irifune and Ohtani, 1986]. After this fluctuation, a sudden jump to high temperature was observed. Possible interpretations of this sudden jump include (1) the local finish of melting because while the heat of fusion was being supplied, the laser power had increased by several steps beyond the power at which the temperature started to fluctuate, the sudden increase in laser power when melting finished locally could have caused a jump in temperature and (2) the lower thermal conductivity of a melt than that of the corresponding solid because the thermal state of the heated area was balanced by the incident laser source and the heat flow away from the spot by the thermal conduction of materials around it, when the melt was created over the heating spot, the relative low thermal conductivity of the melt could have warmed up the heating spot and caused a jump to high temperatures. Therefore the jump to high temperatures could be a consequence of melting of samples.

The magnitude of temperature fluctuation reflected the uncertainty of melting temperature determination. Fluctuations in temperature from ± 50 K to ± 300 K were found in experiments. This uncertainty is larger than the random

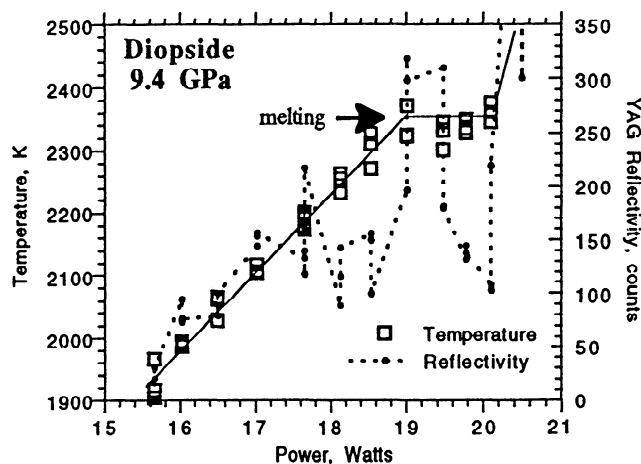


Figure 3. The measured temperature and YAG reflectivity as a function of the laser power at 9.4 GPa for diopside. A clear slope change in temperature and YAG reflectivity appears at the temperatures around 2360 ± 50 K, which is interpreted as the melting of diopside at that pressure. This result is consistent with that determined by multianvil apparatus [Irifune and Ohtani, 1986].

error (± 50 K– ± 100 K) in temperature measurements. The average fluctuation in measured temperature was adopted as the melting temperature without time and spatial correction. The time correction was found to be small due to the use of stable laser source. The spatial correction could be made according to the radial (horizontal) and axial (vertical) temperature gradient (Figure 1). The radial temperature distribution has been discussed above; for example, a positive correction of about 90 K at temperatures of 3150 K is needed to represent the highest temperature of the measured area. There existed also an axial temperature gradient, since the sample was heated by conduction from rhenium metal foil. This gradient is not measurable, however. Numerical calculation [Bodea and Jeanloz, 1989] showed that the temperature distribution is nearly Gaussian in axial direction, and temperature gradients of several hundred degrees per micrometer were predicted with axial dimensions being about 10 μm . In our experiments, we were interested in determining the melting temperature of samples. The highest temperature of a sample was at the interface between the sample and the metal foil, where melting first occurred and the temperature was measured. Therefore the correction for the axial gradient, if any, would be negligible and should be negative. Thus the radial and axial corrections will partly cancel each other. If the amount of axial corrections is larger than that of the radial corrections, our reported melting temperatures would be overestimated by the amount of the difference.

Since solid medium was used in experiments, the sample was under nonhydrostatic stress. The effect of shear stress on melting temperatures is unknown and was not considered in the results.

Experimental Results and Discussion

Inspections

As the laser power was increased, a glow approximately 25 μm in diameter became visible and increased in brightness; at the point corresponding to the temperature fluctuation, the glow started to fluctuate in brightness. After several steps, it became very bright. A clear circular area was observed



Figure 4. Sample of diopside after a melting experiment (run D-2a). The round portion about 25 μm in diameter is the melted area and shows distinctly different optical properties from surroundings. The melted portion is found to be optically anisotropic under polarized light.

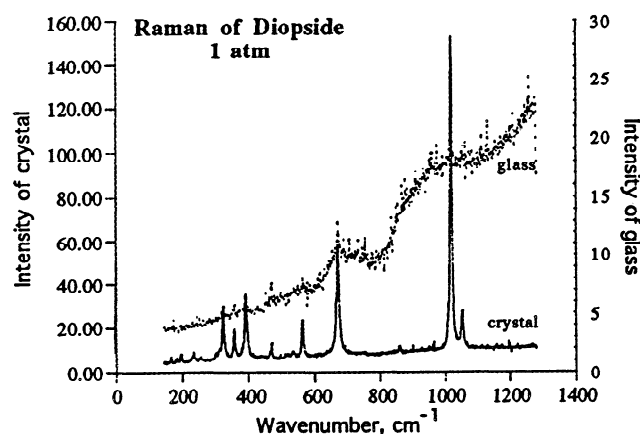


Figure 5. Raman spectra of the diopside sample at heated area and unheated area after an experiment (run D-1a) at ambient pressure. The collection time for both spectra is 5 min with the input 488-nm Ar gas laser power about 50 mW. No baseline correction is made. The spectrum from the unheated area (solid line) is consistent with that of diopside crystalline by *Etchepare* [1972] and *White* [1975], while the spectrum from the laser-heated spot (dots) is the typical glassy feature of diopside [Etchepare, 1972; Dickinson and Scarfe, 1990].

afterward. If the heating was terminated before the bright glow appeared, no clear change in texture was observed afterward.

After quenching from pressure, heated spots were checked in several ways. The heating area turned into a blob which could be optically seen under a microscope as illustrated in Figure 4. The result is shown in Figure 3. Most of the heated areas were found to be optically anisotropic, implying that the melt may not quench to a glass at high pressure. It should be pointed out that the round portion of the sample could be subjected to much higher temperatures than its melting temperature (Figures 2–3). Therefore melting temperature was not determined by the "cook-and-look" method. The purpose of inspections was to characterize the nature of heated spots and melting. Furthermore, the observations confirmed that transparent samples in a YAG laser-heated diamond anvil cell were melted by the metal-contact method.

Micro-Raman spectroscopy was used to check spots before and after heating. For example, a typical feature of a glassy Raman spectrum was observed for diopside at 1 atm after laser heating as shown in Figure 5. However, it was found that the Raman spectrum for diopside at 9.4 GPa after heating did not represent a total glass. The spot showed Raman peaks with less intensity and broader peaks than those before heating (Figure 6). Since the transparent silicate crystal was heated by conduction from the metal, the melting started at the interface between the crystal and the metal. When we measured the Raman on the heated spot, the whole vertical range was covered by the laser beam, the Raman spectra did not conclusively show that diopside melt quenched at high pressure. However, the Raman spectra could be consistent with the findings of *Scarfe and Takahashi* [1986], who found that at pressures of 7–13 GPa, diopside melt does not quench to a glass but exhibits a prismatic quench crystal while diopside melt can be quenched to a glass at < 5 GPa. Raman spectra of laser-heated enstatite, pyrope, stishovite, and corundum quenched from high pressure showed features similar to those of diopside at 9.4 GPa: lower intensity and broader peak

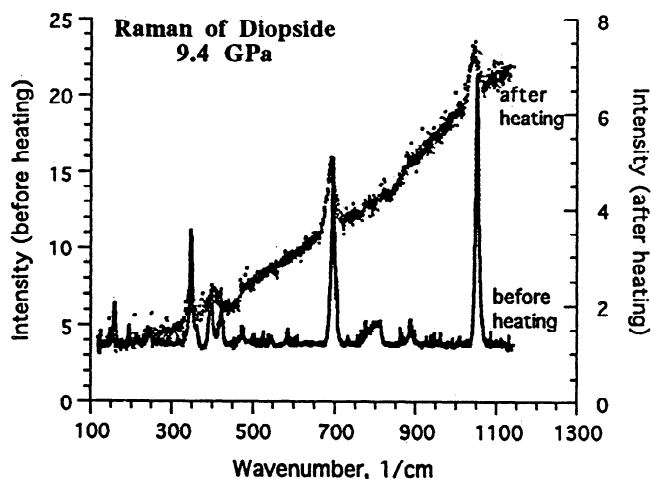


Figure 6. Raman spectra of diopside in a diamond anvil cell before and after a laser-heating experiment (shown in Figure 3) at a pressure of 9.4 GPa. The collection time for both spectra is 15 min with the input 488-nm Ar laser power about 50 mW. A baseline correction is made for the spectrum taken before laser heating but not for that taken after heating. The Raman peaks at the heated area are broader and lower in intensity than those before heating.

widths after heating than before heating. Raman spectra of the wollastonite sample quenched from high pressure showed glassy features on the heated area, while an unheated area, 50 μm away from the heated spot, showed crystalline peaks (Figure 7). The glassy Raman spectrum as shown in Figure 7 is consistent with that of CaSiO_3 glass [Kubicki *et al.*, 1992], which may reflect the non-quenchability of CaSiO_3 perovskite. The Raman bands on unheated area of the quenched sample are broader and lower in intensity than those of the starting wollastonite crystal; moreover, the spectral pattern of

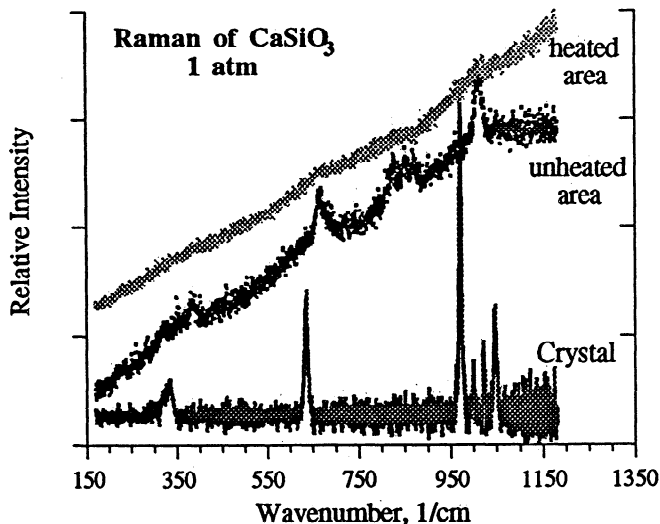


Figure 7. Raman spectra of the starting wollastonite crystal and the quenched sample from about 50 GPa. The collection time for all the spectra is 10 min with the input 488-nm Ar gas laser power about 50 mW. A baseline correction is made for the spectrum of wollastonite crystal but not for those of the heated and unheated area. Note that the Raman bands on the unheated area are different from those of the starting wollastonite crystal.

the unheated area of the quenched sample is different from that of the starting material (see Figure 7), indicating a different crystalline phase from wollastonite. This phase might be assigned to the high-pressure phase of $\text{CaSiO}_3(\text{II})$ (walstromite-like) [Liu and Bassett, 1986; Gasparik *et al.*, 1994].

For stishovite (SiO_2) and corundum (Al_2O_3) it was expected that the melting would be congruent at high pressure. For MgSiO_3 perovskite, Zerr and Boehler [1993] reported congruent melting up to 62.5 GPa. For CaSiO_3 perovskite it was expected that the melting would be congruent at the pressure range of the present study. For diopside, Mao *et al.* [1977], Tamai and Yagi [1988] and Irifune *et al.* [1989] found that diopside decomposes into mixtures of MgSiO_3 components and CaSiO_3 perovskite at pressures above about 18 GPa at 1000°C, whereas Liu [1979, 1987] observed that diopside crystallizes into a cubic perovskite structure of the same composition at 22-23 GPa at 1000°C. For pyrope, Weng *et al.* [1982] determined that at least 25 mol% Al_2O_3 will dissolve in MgSiO_3 perovskite at 40 GPa. To understand the melting nature of diopside and pyrope, electron microprobe analysis was performed for quenched samples.

Mg-rich and Ca-rich phases for diopside sample were found in laser-heated area quenched from high pressures. Figure 8 is one of several back scattering pictures taken from heated spots of diopside quenched from about 50 GPa. Dark areas in the figure contain the MgSiO_3 -rich phase, whereas white areas contain the CaSiO_3 -rich phase. The distribution of elements shows a circular distribution. No rhenium was detectable in either the dark or the white area, which means that chemical contamination of the sample with rhenium metal is not likely. Several very bright spots were found to be concentrations of iron.

The compositions of the unheated, white (not the very bright spots as mentioned above), and dark areas are listed in Table 2 and shown in Figure 9a. The composition of the unheated area is almost the same as that of the starting

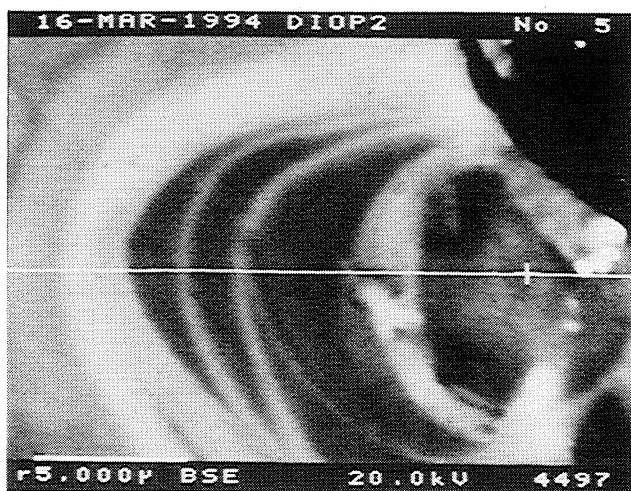


Figure 8. Backscattered electron image of a heated spot of diopside sample. Dark areas correspond to a MgSiO_3 -rich phase, and white areas to CaSiO_3 -rich phase. Several very bright spots were found to be the iron concentration. The dark corner at top right is empty space. The element distributions have been analyzed along the horizontal line from left end to the plus sign (Figure 10).

Table 2. Microprobe Analysis of Quenched Diopside from High P - T

Oxide	unheated	Ca-rich ^a , wt. %	Mg-rich ^b , wt. %
MgO	17.139	6.357	32.523
CaO	25.976	39.666	6.244
SiO ₂	55.726	52.329	59.692
FeO	1.526	0.801	1.778
Total	100.367	99.154	100.252

Sample quenched from pressure about 50 GPa and temperature about 4000 K.

^a The darkest area in Figure 7.

^b The most white area in Figure 7, not the metal spots (see text).

material, suggesting that the breakdown of diopside into Mg-rich and Ca-rich phases needs not only high pressure but also high temperature. The observation of Mg-rich and Ca-rich phases in the heated area was consistent with *Mao et al.* [1977], *Tamai and Yagi* [1988] and *Irifune et al.* [1989]. From the data in Table 2, the solubility of the MgSiO₃ molecule in CaSiO₃ phase is 19 mol%, and the solubility of CaSiO₃ molecule in MgSiO₃ phase was calculated as 12 mol%. These values are larger than those determined by *Irifune et al.* [1989], which may be explained by different experimental conditions. First, the diopside in this study had been subjected to higher pressure and temperature (50 GPa, 4000 K) than that in their sample (24.5 GPa, 1500°C) and the solubility is known to be a function of pressure and temperature. Second, our data represent measurements from the melted area. The solubility could be affected by the melting history and fast quenching in temperature. Qualitatively, the analysis showed that diopside decomposes into a MgSiO₃-rich phase and a CaSiO₃-rich phase at high pressure and temperature.

Since the diopside sample contained 1.5 wt.% of iron oxide (Table 1), the iron partitioning between the coexisting phases has been measured. Figure 10 shows the distributions of three elements (Ca, Mg, Fe) along the horizontal line from the left end to the plus sign in Figure 8. The distributions of Ca and Mg are complementary, while iron preferentially partitions into the Mg-rich phase.

Table 3 lists analyzed compositions of the starting pyrope sample and the heated sample. The composition of the melted

area remained essentially the same as that of the starting pyrope, with slight deficiency in silica (Figure 9b).

To confirm that the solid-solid phase transitions at high pressures had completed in experiments, the heated pyrope sample was studied by X ray diffraction measurements by using synchrotron radiation at Brookhaven National Laboratory. Single perovskite phase was found together with the rhenium metal as shown in Figure 11.

Data Presentation

Experimental results are summarized in Table 4. Pressures from the ruby scale at chosen spots before and after laser heating are reported in columns 3 and 4, respectively. As yet, no satisfactory technique is available to determine the pressure in the diamond anvil cell at high temperatures (>1000 K) during laser heating. The pressure after laser heating plus the estimated thermal pressure was accepted as the pressure on melting. Melting temperatures T_m listed in Table 4 were obtained from the analysis of the laser power/sample temperature function. ΔT in Table 4 reflects the magnitude of temperature fluctuation in slope change range in a power/temperature function.

Melting of MgSiO₃

The experimental results on the melting of MgSiO₃ at pressures up to 41.7 GPa are shown in Figure 12 along with those of *Boyd et al.* [1964], *Presnall and Gasparik* [1990], *Kato and Kumazawa* [1986], *Ito and Katsura* [1992], *Heinz and Jeanloz* [1987], *Knittle and Jeanloz* [1989], *Sweeney and Heinz* [1993] and *Zerr and Boehler* [1993]. Melting temperatures at 6.6 GPa and 9.6 GPa were consistent with the melting curve determined in a piston cylinder by *Boyd et al.* [1964] and in a multianvil apparatus by *Presnall and Gasparik* [1990]. At pressures above 20 GPa, the T_m data are systematically slightly higher than those of *Zerr and Boehler* [1993], but within experimental uncertainties. Melting was characterized by visual observation of convective motion in their experiments, while laser power/sample temperature function was used in the present study. The agreement between their data and ours represents a successful check between those two criteria of melting.

The melting temperatures of *Heinz and Jeanloz* [1987], *Knittle and Jeanloz* [1989], and *Sweeney and Heinz* [1993] lie

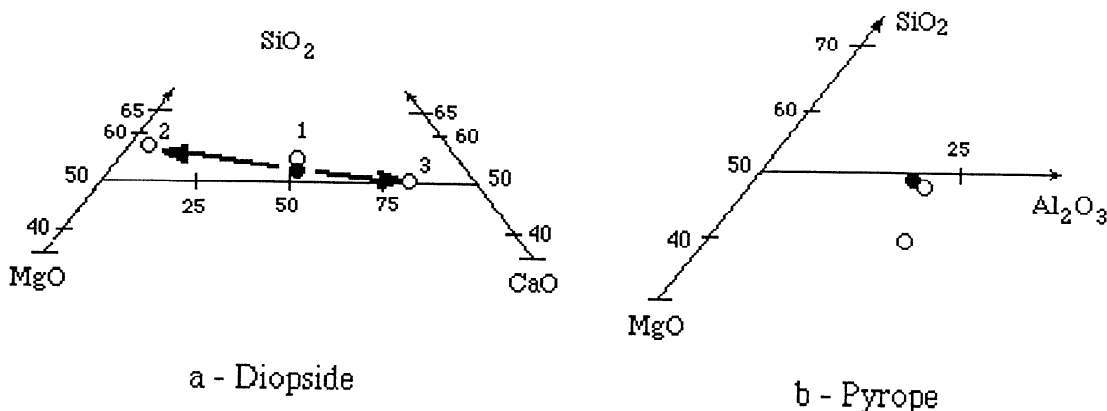


Figure 9. (a) The diopside starting material (solid circle) and quenched sample (open circles) compositions as determined from microprobe analysis. Numbers 1, 2, and 3 indicate the unheated area, the darkest area, and the whitest area, respectively. (b) Pyrope sample compositions at unheated area (solid circle) and heated areas (open circles).

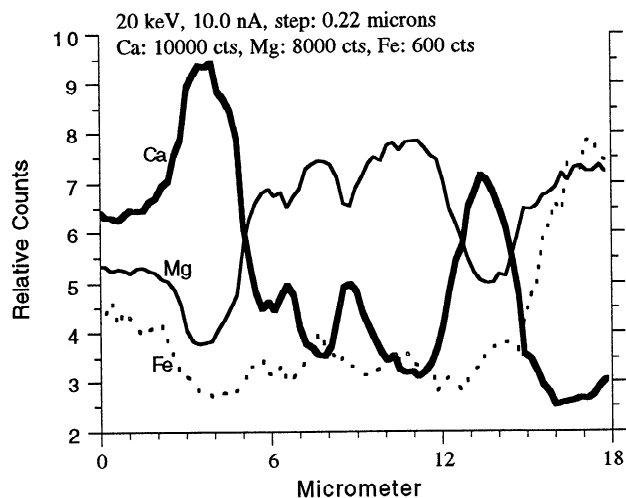


Figure 10. The element (Ca, Mg, Fe) distributions in melted area of diopside sample along the horizontal line from the left end to the plus sign in Figure 8. Measurement conditions are shown in the figure. The distributions of Ca and Mg are complementary, while iron preferentially partitioned into the MgSiO_3 -rich phase.

far below those of *Zerr and Boehler* [1993] and the data of present study. The discrepancy has been discussed by *Zerr and Boehler* [1993], *Heinz et al.* [1994] and *Boehler and Zerr* [1994]. We point out here that melting characterization is critical in determining melting temperature in a laser-heated DAC. Errors in pressure and temperature measurements would be insufficient to explain such a large discrepancy in melting temperature because essentially the same principles were adopted in these measurements [e.g., *Heinz and Jeanloz*, 1987; *Boehler et al.* 1990]. However, adoption of different melting criteria could cause large difference in melting temperature determination. *Heinz and Jeanloz* [1987] employed two methods: first, they bracketed the melting point by measuring the maximum and minimum temperatures obtainable before and after glass formation, respectively; second, they measured the temperature profile across a laser-heated spot and the size of the molten region, and they inferred the temperature corresponding to the crystal-liquid interface as the melting point. In their first cook-and-look method, it is difficult to identify that a heated spot was melted because the quench properties of MgSiO_3 melt at high pressure are still not well understood. *Zerr and Boehler* [1993] observed a silicate perovskite at quenched molten region, while quenched glass blobs were found by *Heinz and Jeanloz* [1987] and *Knittle and Jeanloz* [1989]. In the second method of *Heinz and Jeanloz* [1987], the uncertainty of melting temperature determination

Table 3. Microprobe Analysis of Pyrope Sample

Oxide	Starting Material	Heated area	
		Run P-6a ^a	Run P-6b ^b
MgO	30.900	31.096	38.478
Al_2O_3	23.878	26.044	22.592
SiO_2	44.299	43.105	37.323
Total	99.091	100.245	98.518

^a $P=51.8$ GPa; $T \sim 4500$ K.

^b $P=64.2$ GPa; $T \sim 4500$ K.

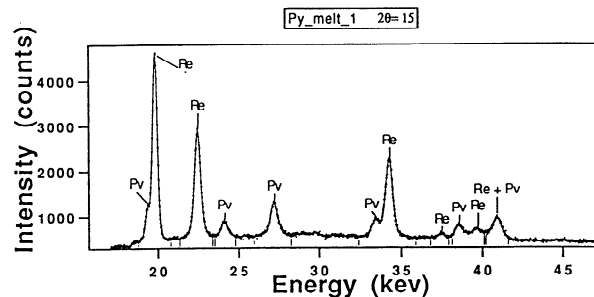


Figure 11. An example of diffraction pattern of the heated pyrope sample after melting experiments (runs P-6a, P-6b). Pv, perovskite.

could be hundreds of degrees to a thousand degrees due to the strong temperature gradient across a heated spot. *Knittle and Jeanloz* [1989] gave no details of how they characterize the liquid and solid phases during laser heating. In the work of *Zerr and Boehler* [1993], in situ visual texture observation was taken to characterize melting. A careful correlation between visual observation and the collected data, together with some experimental experience is necessary for such visual observations because the texture change is small at high pressures. When collected signals are used for melting criteria [*Sweeney and Heinz*, 1993], a series of cross-check experiments are necessary to confirm that the observed anomaly corresponds to melting, because there may exist other possibilities that affect the radiation and reflection from the sample. In the present study, the melting temperatures of diopside, enstatite, pyrope, and ruby determined at ambient pressure and at low pressures by laser power/sample temperature function were found to be consistent with the available data determined by multianvil and other techniques. The anomaly both in power/temperature function and in power/reflectivity function due to melting was clear to recognize; the slope change was usually followed by a big jump in temperature as discussed above. This jump provided an additional indication of melting by the present method.

Melting of $\text{Mg}_3\text{Al}_2\text{Si}_3\text{O}_{12}$

The experimental results on the melting of pyrope sample at pressures up to 64 GPa are shown in Figure 13 along with those of *Irifune and Ohtani* [1986], and *Zhang and Herzberg* [1994]. Our result at 10 GPa was consistent with the melting curve from multianvil apparatus [*Irifune and Ohtani*, 1986; *Zhang and Herzberg*, 1994]. An increase in slope of melting curve at pressures greater than 10 GPa was found by *Zhang and Herzberg* [1994], implying a high melting temperature for pyrope at high pressures. The present high-melting-temperature data support their observation, although a clear slope change at 10 GPa was not resolved in this study.

Boyd and England [1962] have shown that pyrope melts incongruently up to 3.5 GPa. It melts congruently from 3.5 GPa to 16 GPa [*Irifune and Ohtani*, 1986; *Zhang and Herzberg*, 1994]. *Liu* [1977] observed transitions from garnet to ilmenite phase above 25 GPa and subsequently to perovskite phase at pressures above 30 GPa. *Weng et al.* [1982] found that at least 25 mol% of Al_2O_3 is soluble in MgSiO_3 perovskite at 40 GPa. Recently, *FitzGerald et al.* [1994] synthesized $\text{Mg}_3\text{Al}_2\text{Si}_3\text{O}_{12}$ perovskite at 50-70 GPa. Our X ray diffraction data also showed single perovskite phase for the

Table 4. Experimental Results

Run	Sample Starting Composition	P^a GPa	P^b GPa	ΔP^c \pm GPa	T_m^d K	ΔT^e \pm K	Check ^f
E-1a	MgSiO ₃	6.75	6.2	0.5	2320	100	M
E-1b	MgSiO ₃	9.32	9.0	0.7	2450	90	M
E-2a	MgSiO ₃	26.0	22.0	1.5	3020	120	M+R
E-2b	MgSiO ₃	30.5	27.1	2.0	3420	250	M+R
E-2c	MgSiO ₃	33.5	30.5	1.8	3680	180	M+R
E-4a	MgSiO ₃	40.0	37.0	2.5	4000	300	M
E-3a	MgSiO ₃	42.0	39.0	2.5	4050	300	M
W-1a	CaSiO ₃	9.0	7.8	1.0	2275	100	M+R
W-1b	CaSiO ₃	14.0	9.8	0.5	2400	70	M+R
W-2a	CaSiO ₃	18.0	15.5	1.0	2550	150	M
W-1c	CaSiO ₃	19.2	15.8	1.0	2520	80	M+R
W-1d	CaSiO ₃	23.1	19.6	1.2	2680	100	M+R
W-1e	CaSiO ₃	26.5	22.5	2.0	2800	160	M+R
W-2b	CaSiO ₃	28.0	23.1	3.0	2850	200	M
W-2c	CaSiO ₃	34.1	29.4	4.0	3050	300	M
W-3a	CaSiO ₃	36.4	31.5	1.0	3000	200	M+R
W-2d	CaSiO ₃	37.8	32.1	3.0	3090	200	M
W-3b	CaSiO ₃	46.9	40.4	5.0	3500	250	M+R
W-3c	CaSiO ₃	47.1	43.0	5.0	3500	250	M+R
W-3d	CaSiO ₃	51.2	47.1	4.0	3550	150	M+R
W-3e	CaSiO ₃	53.5	48.4	5.0	3650	200	M+R
W-3f	CaSiO ₃	61.4	55.0	4.5	3700	280	M+R
D-1a ^g	CaMgSi ₂ O ₆	0	0	-	1680	50	M+R
D-2a	CaMgSi ₂ O ₆	10.0	8.8	1.0	2390	50	M+R
D-3a	CaMgSi ₂ O ₆	15.6	13.6	1.5	2500	150	M
D-3b	CaMgSi ₂ O ₆	22.7	18.0	2.0	2540	80	M
D-5a	CaMgSi ₂ O ₆	28.0	26.0	1.5	2683	120	M+P
D-4a	CaMgSi ₂ O ₆	29.5	26.7	2.2	2750	80	M+R
D-5b	CaMgSi ₂ O ₆	31.0	30.3	2.0	2750	220	M+P
D-4b	CaMgSi ₂ O ₆	47.0	46.0	2.5	3020	110	M+R
D-6a	CaMgSi ₂ O ₆	54.0	46.7	3.2	3002	150	M+P
D-6b	CaMgSi ₂ O ₆	56.0	54.0	3.0	3050	210	M+P
D-4c	CaMgSi ₂ O ₆	55.0	52.0	2.5	3250	120	M+R
D-6c	CaMgSi ₂ O ₆	67.0	60.0	2.5	3200	140	M+P
D-6d	CaMgSi ₂ O ₆	70.5	65.4	3.0	3400	250	M+P
P-1a	Mg ₃ Al ₂ Si ₃ O ₁₂	8.4	7.8	0.8	2300	80	M+R
P-1b	Mg ₃ Al ₂ Si ₃ O ₁₂	11.0	9.7	1.2	2450	100	M+R
P-2a	Mg ₃ Al ₂ Si ₃ O ₁₂	11.0	10.0	1.0	2480	80	M
P-2b	Mg ₃ Al ₂ Si ₃ O ₁₂	14.0	14.4	1.5	2650	110	M
P-3a	Mg ₃ Al ₂ Si ₃ O ₁₂	22.0	17.5	2.0	2830	150	M
P-2c	Mg ₃ Al ₂ Si ₃ O ₁₂	20.0	18.7	1.6	2800	100	M
P-2d	Mg ₃ Al ₂ Si ₃ O ₁₂	25.0	24.9	2.0	3100	220	M
P-3b	Mg ₃ Al ₂ Si ₃ O ₁₂	28.0	26.0	2.5	3000	130	M
P-4a	Mg ₃ Al ₂ Si ₃ O ₁₂	30.0	28.5	3.0	3270	100	M
P-3d	Mg ₃ Al ₂ Si ₃ O ₁₂	33.0	30.0	3.0	3330	220	M
P-4b	Mg ₃ Al ₂ Si ₃ O ₁₂	38.0	36.9	2.5	3400	120	M
P-4c	Mg ₃ Al ₂ Si ₃ O ₁₂	40.0	38.9	3.2	3500	130	M
P-4d	Mg ₃ Al ₂ Si ₃ O ₁₂	45.0	40.2	2.0	3450	250	M
P-5a	Mg ₃ Al ₂ Si ₃ O ₁₂	45.0	43.0	3.5	3630	120	M
P-5b	Mg ₃ Al ₂ Si ₃ O ₁₂	50.0	44.5	3.0	3750	140	M
P-5c	Mg ₃ Al ₂ Si ₃ O ₁₂	50.5	46.1	2.5	3600	120	M
P-6a	Mg ₃ Al ₂ Si ₃ O ₁₂	52.0	48.4	3.0	3700	300	M+P+S
P-5d	Mg ₃ Al ₂ Si ₃ O ₁₂	55.0	51.9	2.5	3680	150	M
P-5e	Mg ₃ Al ₂ Si ₃ O ₁₂	60.0	54.2	2.5	3700	300	M
P-6b	Mg ₃ Al ₂ Si ₃ O ₁₂	63.0	60.0	3.0	3920	200	M+P+S
Q-1a	SiO ₂	6.5	5.26	.6	2750	100	M+R
Q-1b	SiO ₂	9.0	8.6	1.0	2900	70	M+R
S-1a	SiO ₂	15.0	14.9	1.0	3400	130	M+R
S-1b	SiO ₂	18.0	15.5	1.3	3450	120	M+R
S-2a	SiO ₂	22.0	20.5	2.0	3900	150	M
S-2b	SiO ₂	25.0	23.7	1.5	4100	180	M
S-2c	SiO ₂	27.0	24.0	2.0	3950	180	M
S-3a	SiO ₂	30.0	29.0	1.0	4100	280	M
S-3b	SiO ₂	37.0	34.0	2.0	4250	200	M
R-1a ^g	Al ₂ O ₃	0	0	-	2350	50	M+R
R-2a	Al ₂ O ₃	1.5	1.0	0.3	2430	80	M+R
R-2b	Al ₂ O ₃	7.0	6.5	0.8	3030	100	M+R
R-2c	Al ₂ O ₃	9.0	8.4	1.0	3135	200	M+R
R-3a	Al ₂ O ₃	15.5	14.3	1.2	3290	120	M
R-4a	Al ₂ O ₃	18.0	15.6	1.5	3380	150	M

Table 4. (continued)

Run	Sample Starting Composition	P^a GPa	P^b GPa	ΔP^c \pm GPa	T_m^d K	ΔT^e \pm K	Check ^f
R-3b	Al ₂ O ₃	18.0	16.2	1.5	3440	250	M
R-3c	Al ₂ O ₃	21.0	19.5	2.0	3495	120	M
R-4b	Al ₂ O ₃	25.0	23.2	2.0	3525	120	M
R-4c	Al ₂ O ₃	27.5	23.7	2.0	3600	180	M

^a Pressure of the chosen spot before laser heating.

^b Pressure measured immediately after laser heating.

^c Pressure gradient measured in 10 μ m across the heated spot.

^d Temperature at fluctuation range in laser/sample temperature function; no correction was made.

^e Magnitude of temperature fluctuation; The value does not include the error in temperature measurements (see text).

^f Method used for checking quenched samples: M, microscope; R, Raman spectroscopy; P, electron microprobe; S, synchrotron X ray diffraction.

^g The melting measurement at 1 atm was carried out outside the diamond anvils under argon flow.

heated pyrope sample (see Figure 11). Thus perovskite solid solution exists in $(1-x)\text{MgSiO}_3 \cdot x\text{Al}_2\text{O}_3$ with x at least to 0.25. However, phase transitions at high pressure have not been studied for the range with $x > 0.25$; the solubility limit of Al₂O₃ in MgSiO₃ perovskite at high pressure is still uncertain. If the solubility of Al₂O₃ in MgSiO₃ perovskite were limited to 25 mol%, then the experimental results on melting pyrope sample above 30 GPa would represent the melting of Mg₃Al₂Si₃O₁₂ perovskite. However, it is likely that more than 25 mol% Al₂O₃ is soluble in MgSiO₃ perovskite. Then the present result would represent the melting of a solid solution. For a solid solution, Mg₃Al₂Si₃O₁₂ would melt over a temperature interval with a variable composition of melts. The composition of the first-

formed liquid would be rich in Al₂O₃ and deficient in SiO₂. Microprobe analysis of the melted area showed it to be deficient in silica and slightly excess alumina, as expected. Since the heating spot may have experienced higher temperatures than melting, as was discussed, the analyzed data may not represent the composition of the melt in the solidus-liquidus region. The melt composition could not be determined accurately in the present study. The present experimental points could be a representation of the whole temperature interval of the solid solution Mg₃Al₂Si₃O₁₂.

Melting of CaMgSi₂O₆ and CaSiO₃

The experimental results on melting with the starting composition of CaMgSi₂O₆ to pressures up to 70 GPa are shown in Figure 14 along with those of Williams and Kennedy [1969], Scarfe and Takahashi [1986], and Irifune and Ohtani [1986]. Our result at 9.4 GPa is consistent with the melting curve from multianvil apparatus [Irifune and Ohtani, 1986]. The data of Boyd and England [1963] and Boettcher et al. [1982] are also consistent with our data within experimental uncertainties (not shown in Figure 14 for clarity).

Phase transformations in diopside at high pressures have been studied by many researchers. Liu [1979, 1987] observed

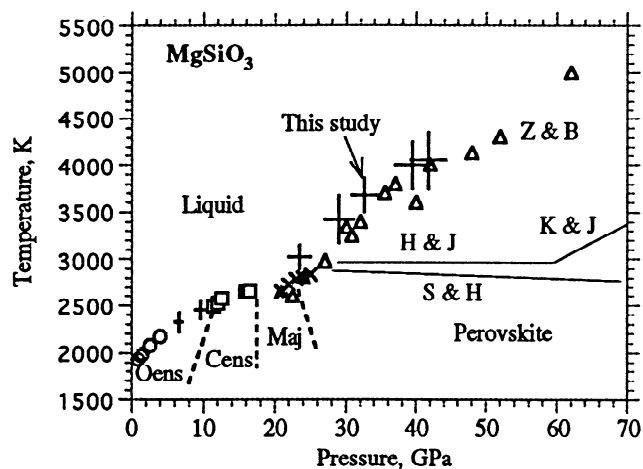


Figure 12. Experimental results for melting of MgSiO₃: circles, Boyd et al. [1964]; squares, Presnall and Gasparik [1990]; crosses, Ito and Katsura [1992]; solid triangle, Kato and Kumuzawa [1986]; open triangles, Zerr and Boehler [1993]; pluses, this study. Lines as noted in the figure are H & J, Heinz and Jeanloz [1987]; K & J, Knittle and Jeanloz [1989]; S & H, Sweeney and Heinz [1993]. Melting temperatures in this study are obtained by plotting the laser power/sample temperature functions. Pressures are those measured after laser heating plus thermal pressure estimation (7%). Vertical bars represent the magnitude of temperature fluctuation in the slope change range. Horizontal bars represent the pressure gradient in 10 μ m across the heated spot. Polymorphs of MgSiO₃ were shown: Oens, orthoenstatite; Cens, clinoenstatite; Maj, majorite.

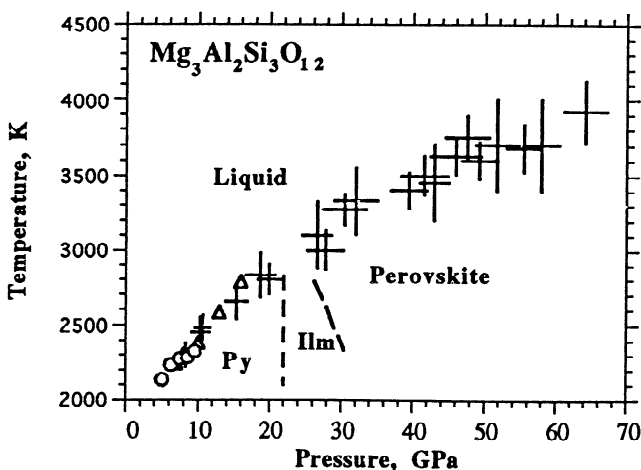


Figure 13. Experimental results for melting of Mg₃Al₂Si₃O₁₂: circles, Irifune and Ohtani [1986]; triangles, Zhang and Herzberg [1994]; pluses, this study. The size of the pluses represents the uncertainty in pressure and temperature. Py, pyrope; Ilm, ilmenite.

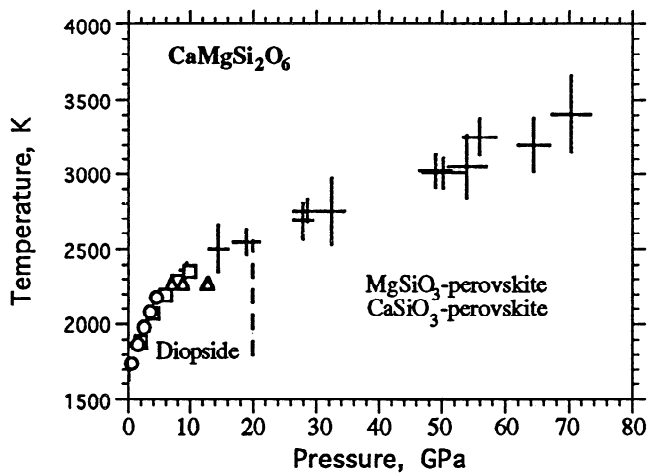


Figure 14. Experimental results for melting of $\text{CaMgSi}_2\text{O}_6$: circles, Williams and Kennedy [1969]; squares, Irifune and Ohtani [1986]; triangles, Scarfe and Takahashi [1986]; pluses, this study. The size of bars represents the uncertainty in pressure and temperature.

that diopside crystallizes into a cubic perovskite structure of the same composition at 22–23 GPa at 1000°C; Mao *et al.* [1977], Tamai and Yagi [1988], and Irifune *et al.* [1989] found that diopside decomposes into mixtures of MgSiO_3 components and CaSiO_3 perovskite at pressures above about 18 GPa at 1000°–1500°C. We found that the quenched samples contained a MgSiO_3 -rich phase and a CaSiO_3 -rich phase in the molten areas. Therefore the melting mode of $\text{CaMgSi}_2\text{O}_6$ composition would be the eutectic melting of MgSiO_3 components and CaSiO_3 perovskite above pressures at about 20 GPa. The eutectic melting temperature reflects the minimum melting temperature of MgSiO_3 - CaSiO_3 join at high pressure. The present result for the diopside sample at pressures above 20 GPa may be used to represent the eutectic melting, although the melting temperature determined may be slightly higher than the eutectic temperature due to difficulties arising from the melting experiments of multicomponent systems in a diamond anvil cell (the samples could be non-uniform on a

scale of micrometers and temperature gradients could lead to unmixing during heating). As shown in Figure 14, the representative melting temperatures of MgSiO_3 - CaSiO_3 perovskites increase steadily with increasing pressure ($dT_m/dP = 14 \pm 4$ K/GPa over the pressure range of 20–70 GPa).

The experimental results for melting of CaSiO_3 composition to pressures of 60 GPa are shown in Figure 15 along with the results of Gasparik *et al.* [1994]. Phase transition studies at high pressure showed that wollastonite transforms to high-pressure $\text{CaSiO}_3(\text{II})$ (walstromite-like) phase above 3 GPa [e.g., Gasparik *et al.*, 1994], and to cubic perovskite phase at pressures above about 11 GPa [e.g., Gasparik *et al.*, 1994]. Gasparik *et al.* [1994] observed that the melting temperature for CaSiO_3 perovskite increased sharply by 360 K in the pressure interval of 13.5–15.2 GPa. Because of the limited two melting points at pressures below 15 GPa in this study, it is difficult to have a direct comparison in melting slope with theirs. However, our data at pressures above 15 GPa imply that the unusually deep dT_m/dP slope for CaSiO_3 perovskite [Gasparik *et al.*, 1994] would flatten out at high pressures.

Melting of SiO_2

Melting of silica has been reported by Jackson [1976], Kanzaki [1990], and recently by Zhang *et al.* [1993]. A series of shock wave measurements on single-crystal and fused quartz were made to determine melting temperatures of stishovite at high pressures [Ahrens *et al.*, 1982; Kondo *et al.*, 1983; Lyzenga *et al.*, 1983; Schmitt and Ahrens, 1989]. Our melting data on silica are shown in Figure 16 along with reported data. Our results at 5.6 GPa and 9.2 GPa are consistent with those of Kanzaki [1990] and Zhang *et al.* [1993]. Shock wave data on melting of stishovite are quite scattered. Our melting temperatures for stishovite at 15–37 GPa are higher than those determined by Schmitt and Ahrens [1989]. When extrapolating our data to high pressures, they are in reasonable agreement with the melting point (T_m of 4500 K at 70 GPa) by Lyzenga *et al.*, [1983].

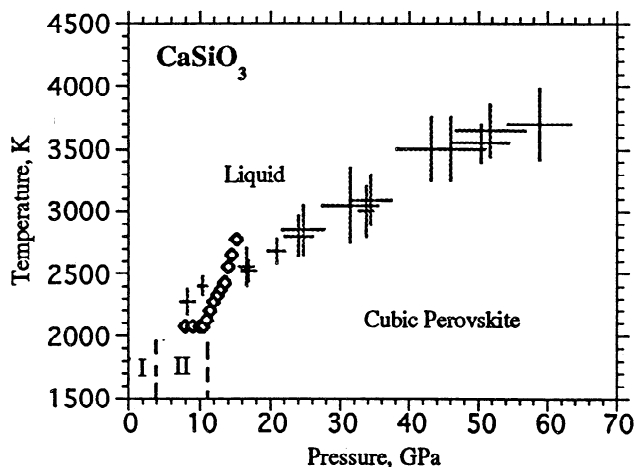


Figure 15. Experimental results for melting of CaSiO_3 : triangles, Gasparik *et al.* [1994]; pluses, this study. The size of bars represents the uncertainty in pressure and temperature. I, wollastonite; II, walstromite-like phase.

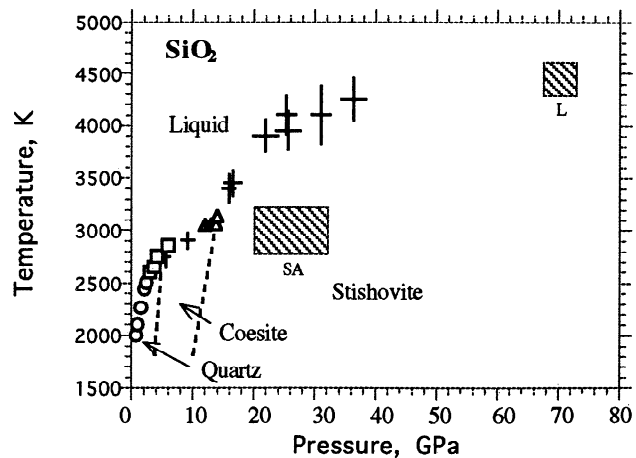


Figure 16. Melting results for silica: circles, Jackson [1976]; squares, Kanzaki, [1990]; triangles, Zhang *et al.* [1993]; pluses, this study. The size of bars represents the uncertainty in pressure and temperature. Shock wave data on melting of stishovite are scattered. The data of Schmitt and Ahrens [1989] (SA) and Lyzenga *et al.* [1983] (L) are shown.

Before choosing stishovite as a starting material, we used quartz as a sample. At pressures of 5.6 GPa and 9.2 GPa, melting temperatures were determined as 2750 K and 2900 K, respectively. However, at pressures from 10 GPa to 25 GPa, we found that temperatures started to fluctuate at around 1500-2000 K (inferred as low-temperature fluctuation) and then jumped to above 4000 K. The effect disappeared at pressures above 25 GPa. Therefore melting temperature measurements with the present technique over the pressure range of 10-25 GPa were not possible with quartz as a starting material. Since this low-temperature fluctuation was not observed for other samples in the present study, the effect may be associated with the properties of quartz over the pressure range of 10-25 GPa. Possible interpretations for the low temperature fluctuation are (1) phase transition of coesite to stishovite at 10-13 GPa [Yagi and Akimoto, 1976; Zhang *et al.*, 1993; Serghiou *et al.*, 1995] and (2) amorphization of quartz or coesite over the pressure range [e.g., Hemley *et al.*, 1988].

The present melting data at pressures above 15 GPa were measured using synthetic stishovite as a starting sample. According to our melting data, accurate determination of the liquid-coesite-stishovite triple point was difficult due to limited experimental runs and melting temperature uncertainties. As is shown in Figure 17, if the triple point determined by Zhang *et al.* [1993] was adopted, the melting slope, dT_m/dP , for stishovite above the triple point would be as large as 100 ± 20 K/GPa over the pressure range 13.5 - 23 GPa. At pressure greater than 23 GPa, our data showed that the slope flattens to 30 ± 10 K/GPa. Recently, Serghiou *et al.* [1995] measured the coesite-stishovite transition in a CO₂ laser-heated diamond cell and suggested a boundary curve in agreement with Yagi and Akimoto's [1976]. If their coesite-stishovite boundary was adopted, the slope change across the triple point would be slightly smoothed out (Figure 17).

Melting of Al₂O₃

There are no reported high-pressure melting data for corundum to our knowledge. Figure 18 showed measured melting temperatures to a pressure of 25.4 GPa. Melting of corundum provides an end-member constraint in modeling the

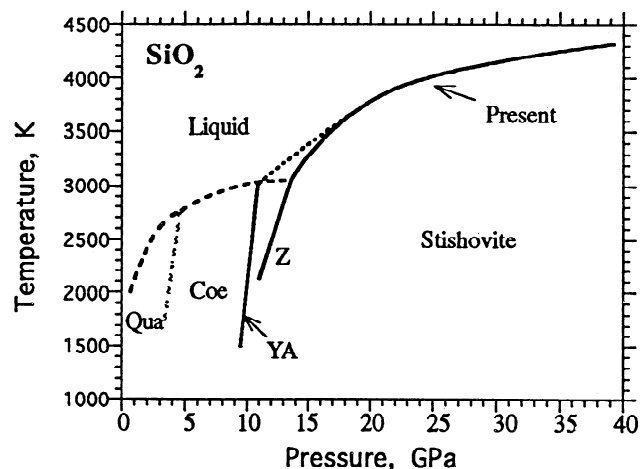


Figure 17. A review of silica phase diagram. Initial melting slope of stishovite above the coesite-stishovite-liquid triple point depends on the location of the triple point. Z, Zhang *et al.* [1993]; YA, Yagi and Akimoto, [1976]; Qua, quartz; Coe, coesite.

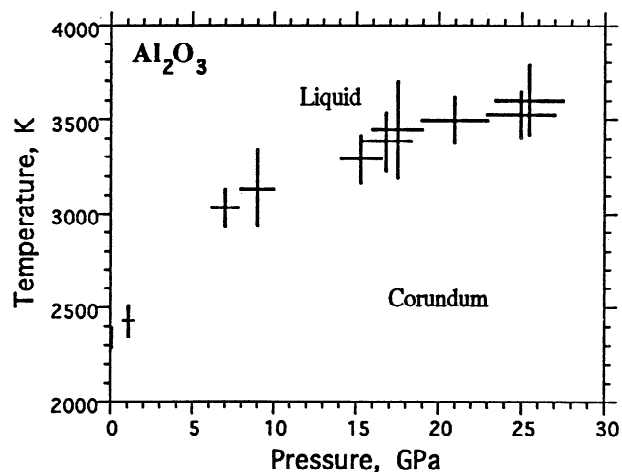


Figure 18. Experimental results for melting of ruby. The size of the symbols represents the uncertainty in pressure and temperature.

melting relation in systems containing Al₂O₃ component. Technically, understanding of high pressure melting of corundum is important, because in many melting experiments, corundum was used as thermal isolation material and pressure medium [e.g., Williams and Jeanloz, 1991; Boehler 1993; Saxena *et al.*, 1994]. Present data showed that melting temperatures of corundum are higher than those of iron, nickel, and cobalt [P. Lazor and G. Shen, unpublished manuscript, 1994]. Therefore, the use of corundum will not affect the determination of melting temperatures for iron group metals unless there is a reaction.

Melting Relations in the Lower Mantle

The lower mantle may consist of silicate perovskites and magnesiowüstite [Liu, 1976; Mao *et al.*, 1977; Knittle and Jeanloz, 1987; Ito and Takahashi, 1989]. Figure 19 summarizes melting curves of some lower mantle minerals. All these solids were found to be highly refractory requiring high temperatures for melting at lower mantle pressures. The high melting temperatures and positive dT_m/dP slopes of three perovskites (MgSiO₃, CaSiO₃, Mg₃Al₂Si₃O₁₂) may indicate a high melting temperature in the lower mantle.

The mantle rocks are believed to be composed of a mixture of crystalline phases. Melting temperatures and melting slopes of CaSiO₃ and Mg₃Al₂Si₃O₁₂ perovskites were found to be less than those of MgSiO₃ perovskite (Figure 19), suggesting that the presence of Ca, Al elements will lower the melting temperature in the lower mantle estimated by the melting of MgSiO₃ perovskite and that this effect would increase with increasing pressures. The magnitude of the effect depends on the compositional and mineralogical model of the mantle and melting modes of MgSiO₃-CaSiO₃ system and MgSiO₃-Al₂O₃ system at high pressures. The MgSiO₃ and CaSiO₃ perovskite were found to be immiscible and the minimum melting temperatures of the system MgSiO₃-CaSiO₃ at lower mantle pressures are expressed by the eutectic melting temperatures. Al₂O₃ was found to be soluble in MgSiO₃ perovskite forming solid solutions, and melting temperatures of MgSiO₃ perovskite will be lowered by the presence of Al. The magnitude of the reduction depends on Al content in the lower mantle, which is expected to be low [Anderson, 1989].

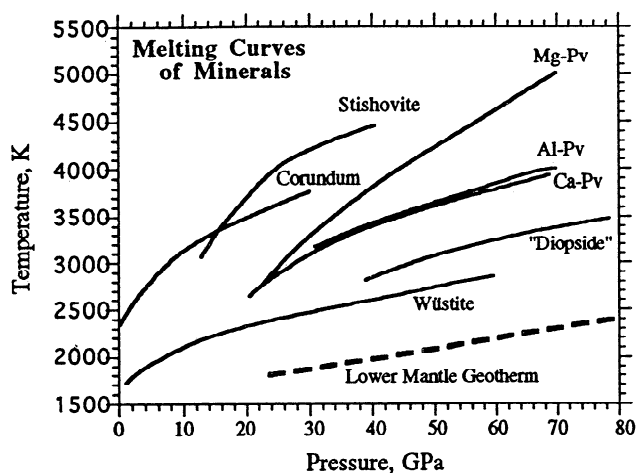


Figure 19. A summary of melting curves of some lower mantle minerals. The curves were plotted using third-order polynomial equations for interpolation, fitted by least squares to the experimental data of melting. Melting of MgSiO_3 perovskite (Mg-Pv) from Zerr and Boehler [1993] and this study; melting of CaSiO_3 perovskite (Ca-Pv), stishovite, and corundum from this study; melting of wüstite from Shen *et al.* [1993]. Al-Pv and "diopside" curves denote the melting results on pyrope and diopside samples, respectively (see text for more discussions). An approximate mantle geothermal [Shankland and Brown, 1985] was plotted as a dashed line for comparison.

However, since the melting slope, dT_m/dP , determined from the pyrope sample is less than that of MgSiO_3 perovskite, the effect of Al on melting of Mg-perovskite will increase with increasing pressure. At deep lower mantle pressures the effect might be considerable.

It needs to be pointed out that Al and Ca may be incorporated in certain other phases, which include a high-pressure form of MgAl_2O_4 [Irfune *et al.*, 1991], a form of $(\text{Ca,Mg})\text{Al}_2\text{Si}_2\text{O}_8$ with the hollandite structure [Maddon *et al.*, 1989], $\text{Ca}_2\text{AlSiO}_{5.5}$ with a rhombohedral perovskite structure [FitzGerald and Ringwood, 1991], and Al_2SiO_5 with a V_3O_5 structure [Ahmed-Zaid and Madon, 1991]. Thus more phase transition studies and melting measurements are required to better understand the effect of the presence of Al_2O_3 and CaO components on the melting relations in the lower mantle. Very recently, Irfune [1994] reported an experimental study of phase transformations in a pyrolite mantle composition in a pressure interval of 23-28 GPa and concluded that Al_2O_3 is accommodated mainly in MgSiO_3 perovskite; no separate aluminum phase was observed, while a separate CaSiO_3 perovskite was observed along with MgSiO_3 perovskite and magnesiowüstite.

The iron component will also affect the melting temperature of MgSiO_3 perovskite. However, no measurement was made in this study on the effects of Fe on melting because of the Soret diffusion effect of Fe in a laser heating spot as found by Heinz and Jeanloz [1987]. Zerr and Boehler [1993] determined the melting temperatures of $(\text{Mg}_{0.88}\text{Fe}_{0.12})\text{SiO}_3$ perovskite to 60 GPa, and no significant difference was found in melting temperature from that of MgSiO_3 perovskite within experimental uncertainties. One may conclude that the presence of Fe and Al will not significantly affect the melting temperature of MgSiO_3 perovskite. Whereas the Fe, Al effect would be larger at higher pressures; when the melting curve is

extrapolated to the pressure of core-mantle boundary, Fe and Al effects should be considered. The presence of Ca may reduce the melting temperature of MgSiO_3 perovskite because of the eutectic melting nature of CaSiO_3 - MgSiO_3 system at high pressure. Quantitative analysis can not be made until more melting data of $(\text{Mg,Fe,Al})(\text{Si,Al})\text{O}_3$ perovskite at very high pressures and more accurate knowledge of phase transitions and Fe, Ca and Al chemistry in the lower mantle are available.

Although free SiO_2 and Al_2O_3 most likely do not exist in substantial quantities in the lower mantle, they are constituents of silicate perovskites. The present data provided an end-member input in modeling the melting relations of the FeO - CaO - Al_2O_3 - MgO - SiO_2 system, which represents the lower mantle chemistry.

Acknowledgments. We are grateful to S. K. Saxena for many suggestions and comments. G.S. thanks H. K. Mao and R. J. Hemley for critical comments on the manuscript, P. Nysten for providing the diopside sample, H. Skogby for providing the orthoenstatite crystal, H. Harryson for helping electron-microprobe measurements, and J. Hu for help in synchrotron measurements. Samples of stishovite and pyrope were synthesized at Stony Brook and kindly provided by R. Liebermann and J. Zhang. We are grateful for thoughtful reviews by David Walker, one anonymous reviewer, and one Associate Editor. The work was supported by grants (to S. K. Saxena) from the Swedish Natural Science Research Council (NFR) and Wallenbergs Foundation. This work was submitted to Uppsala University in partial fulfillment of a doctoral thesis.

References

- Ahmed-Zaid, I., and M. Madon, A high-pressure form of Al_2SiO_5 as a possible host of aluminium in the lower mantle, *Nature*, 353, 426-428, 1991.
- Ahrens, T. J., G. A. Lyzenga, and A. C. Mitchell, Temperatures induced by shock waves in minerals: Applications to geophysics, in *High Pressure Research in Geophysics*, edited by S. Akimoto and M. H. Manghnani, pp. 579-594, Cent. for Acad. Publ., Tokyo, 1982.
- Anderson, D. L., *Theory of the Earth*, Blackwell Sci., Cambridge, Mass., 1989.
- Bodea, S., and R. Jeanloz, Model calculations of the temperature distribution in the laser-heated diamond cell, *J. Appl. Phys.*, 65, 4688-4692, 1989.
- Boehler, R., Melting of the Fe-FeO and Fe-FeS systems at high pressures: Constraints on core temperatures, *Earth Planet. Sci. Lett.*, 111, 217-227, 1992.
- Boehler, R., Temperatures in the Earth's core from melting-point measurements of iron at high static pressures, *Nature*, 363, 534-536, 1993.
- Boehler, R., and A. Chopelas, Phase transitions in a 500 kbar - 3000 K gas apparatus, in *High-Pressure Research: Application to Earth and Planetary Sciences, Geophys. Monogr. Ser.*, vol. 67, edited by Y. Syono and M. H. Manghnani, pp. 55-60, AGU, Washington, D. C., 1992.
- Boehler, R., and A. Zerr, Response to: High-pressure melting of $(\text{Mg,Fe})\text{SiO}_3$ -perovskite, *Science*, 264, 280-281, 1994.
- Boehler, R., N. von Bargen, and A. Chopelas, Melting, thermal expansion, and phase transitions of iron at high pressures, *J. Geophys. Res.* 95, 21,731-21,736, 1990.
- Boettcher, A. L., C. W. Burnham, K. E. Windom, and S. R. Bohlen, Liquids, glasses and the melting of silicates to high pressures, *J. Geol.*, 90, 127-138, 1982.
- Boyd, F. R., and J. L. England, Mantle minerals, *Year Book Carnegie Inst. Wash.*, 61, 107-112, 1962.
- Boyd, F. R., and J. L. England, Effect of pressure on the melting of diopside, $\text{CaMgSi}_2\text{O}_6$, and albite, $\text{NaAlSi}_3\text{O}_8$, in the range up to 50 kilobars, *J. Geophys. Res.*, 68, 311-323, 1963.
- Boyd, F. R., J. L. England, and B. T. C. Davis, Effects of Pressure on the melting and polymorphism of enstatite, MgSiO_3 , *J. Geophys. Res.*, 69, 2101-2109, 1964.
- Cabannes, F. Facteurs de réflexion et d'émission des métaux, *J. Phys.*, 28, 235-248, 1967.
- Clark, G. L., *The Encyclopedia of Chemistry*, 2nd ed., Reinhold., New York, 1952.

- Dickinson, J. E., Jr., and C. M. Scarfe, Raman spectroscopic study of glasses on the join diopside-albite, *Geochim. Cosmochim. Acta*, **54**, 1037-1043, 1990.
- Etchepare, J., Study by Raman spectroscopy of crystalline and glassy diopside, in *Amorphous Materials*, edited by R. W. Douglas and B. Ellis, pp. 337-346, John Wiley, New York, 1972.
- FitzGerald, J. D., and A. E. Ringwood, High pressure rhombohedral perovskite phase $\text{Ca}_2\text{AlSiO}_{5,5}$, *Phys. Chem. Mineral.*, **18**, 40-46, 1991.
- FitzGerald, J. D., S. Kesson, J. M. Shelley, and R. L. Withers, Structure and crystal chemistry of aluminum magnesian silicate perovskites, and perovskites along the join pyrope-almandine (abstract), *Eos Trans. AGU*, **75**(16), Spring Meet. Suppl., 339, 1994.
- Gasparik, T., K. Wolf, and C. M. Smith, Experimental determination of phase relations in the CaSiO_3 system from 8 to 15 GPa, *Am. Mineral.*, **79**, 1219-1222, 1994.
- Heinz, D. L., Thermal pressure in the laser-heated diamond anvil cell, *Geophys. Res. Lett.*, **17**, 1161-1164, 1990.
- Heinz, D. L., and R. Jeanloz, Measurement of the melting curve of $\text{Mg}_{0.9}\text{Fe}_{0.1}\text{SiO}_3$ at lower mantle conditions and its geophysical implications, *J. Geophys. Res.*, **92**, 11,437-11,444, 1987.
- Heinz, D. L., and J. S. Sweeney, Quantitative temperature measurement in the laser-heated diamond anvil cell (abstract), *Eos Trans. AGU*, **73**(43), Fall Meet. suppl., 579, 1992.
- Heinz, D. L., J. S. Sweeney, and P. Miller, A laser heating system that stabilizes and controls the temperature: Diamond anvil cell applications, *Rev. Sci. Instrum.*, **62**, 1568-1575, 1991.
- Heinz, D. L., E. Knittle, J. F. Sweeney, Q. Williams, and R. Jeanloz, High-pressure melting of $(\text{Mg,Fe})\text{SiO}_3$ -perovskite, *Science*, **264**, 279-280, 1994.
- Hemley, R. J., A. P. Jephcoat, H. K. Mao, L. C. Ming, and M. H. Manghnani, Pressure-induced amorphization of crystalline silica, *Nature*, **334**, 52-54, 1988.
- Irifune, T., Absence of an aluminous phase in the upper part of the Earth's lower mantle, *Nature*, **370**, 131-133, 1994.
- Irifune, T. and E. Ohtani, Melting of pyrope $\text{Mg}_3\text{Al}_2\text{Si}_2\text{O}_{12}$ up to 10 GPa: Possibility of a pressure-induced structural change in pyrope melt, *J. Geophys. Res.*, **91**, 9357-9366, 1986.
- Irifune, T., and A. E. Ringwood, Phase transformations in a harzburgite composition to 26 GPa: implications for dynamical behaviour of the subducting slab, *Earth Planet. Sci. Lett.*, **86**, 365-376, 1987.
- Irifune, T., J. Susaki, T. Yagi, and H. Sawamoto, Phase transformations in diopside $\text{CaMgSi}_2\text{O}_6$ at pressures up to 25 GPa, *Geophys. Res. Lett.*, **16**, 187-190, 1989.
- Irifune, T., K. Fujino, and E. Ohtani, A new high-pressure form of MgAl_2O_4 , *Nature*, **349**, 409-411, 1991.
- Ito, E., and T. Katsura, Melting of ferromagnesian silicates under the lower mantle conditions, in *High-Pressure Research: Application to Earth and Planetary Sciences*, *Geophys. Monogr. Ser.*, vol. 67, edited by Y. Syono and M. H. Manghnani, pp. 315-322, AGU, Washington, D. C., 1992.
- Ito, E., and E. Takahashi, Postspinel transformations in the system Mg_2SiO_4 - Fe_2SiO_4 and some geophysical implications, *J. Geophys. Res.*, **94**, 10,637-10,646, 1989.
- Jackson, I., Melting of silica isotypes SiO_2 , BeF_2 and GeO_2 at elevated pressures, *Phys. Earth Planet. Inter.*, **13**, 218-231, 1976.
- Kanzaki, M., Melting of silica up to 7 GPa, *J. Am. Ceram. Soc.*, **73**, 3706-3707, 1990.
- Kato, T., and M. Kumazawa, Melting and phase relations in the system Mg_2SiO_4 - MgSiO_3 at 20 GPa under hydrous conditions, *J. Geophys. Res.*, **91**, 9351-9355, 1986.
- Knittle, E., and R. Jeanloz, Synthesis and equation of state of $(\text{Mg,Fe})\text{SiO}_3$ perovskite to over 100 gigapascals, *Science*, **235**, 668-670, 1987.
- Knittle, E., and R. Jeanloz, Melting curve of $(\text{Mg,Fe})\text{SiO}_3$ perovskite to 96 GPa: Evidence for a structural transition in lower mantle melts, *Geophys. Res. Lett.*, **16**, 421-424, 1989.
- Kondo, K., T. J. Ahrens, and A. Sawaoka, Shock induced spectra of fused quartz, *J. Appl. Phys.*, **54**, 4382-4385, 1983.
- Kubicki, J. D., R. J. Hemley, and A. M. Hofmeister, Raman and infrared study of pressure-induced structural changes in MgSiO_3 , $\text{CaMgSi}_2\text{O}_6$, and CaSiO_3 glasses, *Am. Mineral.*, **77**, 258-269, 1992.
- Lazor, P., G. Shen, and S. K. Saxena, Laser-heated diamond anvil cell experiments at high pressure: Melting of nickel up to 700 kbar, *Phys. Chem. Mineral.*, **20**, 86-90, 1993.
- Liu, L.G., Orthorhombic perovskite phases observed in olivine, pyroxene and garnet at high pressures and temperatures, *Phys. Earth Planet. Inter.*, **11**, 289-298, 1976.
- Liu, L. G., The system enstatite-pyrope at high pressures and temperatures and the mineralogy of the Earth's mantle, *Earth Planet Sci Lett.*, **36**, 237-245, 1977.
- Liu, L. G., The system enstatite-wollastonite at high pressure and temperature, with emphasis on diopside, *Phys. Earth Planet. Inter.*, **19**, 15-18, 1979.
- Liu, L. G., New silicate perovskites, *Geophys. Res. Lett.*, **14**, 1079-82, 1987.
- Liu, L. G., and W. A. Bassett, *Elements, Oxides, Silicates: High-Pressure Phases with Implications for the Earth's Interior*, *Oxford Monogr. Geol. Geophys.* vol. 4, Oxford Univ. Press, New York, 1986.
- Lyzenga, G. A., T. J. Ahrens, and A. C. Mitchell, Shock temperatures of SiO_2 and their geophysical implications, *J. Geophys. Res.*, **88**, 2431-2444, 1983.
- Madon, M., J. Castex, and J. Peyronneau, A new aluminocalcic high-pressure phase as a possible host of calcium and aluminium in the lower mantle, *Nature*, **342**, 422-424, 1989.
- Mao, H. K., J. Xu, and P. M. Bell, Calibration of the ruby pressure gauge to 800 kbar under quasi-hydrostatic conditions, *J. Geophys. Res.*, **91**, 4673-4676, 1986.
- Mao, H. K., T. Yagi, and P. M. Bell, Mineralogy of the Earth's deep mantle: Quenching experiments of mineral compositions at high pressure and temperature, *Year Book Carnegie Inst. Wash.*, **76**, 502-504, 1977.
- Mao, H. K., P. M. Bell, J. W. Shaner, and D. J. Steinberg, Specific volume measurements of Cu, Mo, Pd and Au and calibration of the ruby R1 fluorescence pressure gauge for 0.06 to 1 Mbar, *J. Appl. Phys.*, **49**, 3276-83, 1978.
- Mao, H. K., L. C. Chen, R. J. Hemley, A. P. Jephcoat, and Y. Wu, Stability and equation of state of CaSiO_3 -perovskite to 134 GPa, *J. Geophys. Res.*, **94**, 17,889-17,894, 1989.
- O'Neil, B., and R. Jeanloz, Experimental petrology of the lower mantle: A natural peridotite taken to 54 GPa, *Geophys. Res. Lett.*, **17**, 1477-1480, 1990.
- Presnall, D. C., and T. Gasparik, Melting of enstatite from 10 to 16.5 GPa, the beta phase-majorite eutectic at 16.5 GPa, and implications for the origin of the mantle, *J. Geophys. Res.*, **95**, 15,771-15,777, 1990.
- Saxena, S. K., G. Shen, and P. Lazor, Experimental evidence for a new iron phase and implications for Earth's core, *Science*, **260**, 1312-1314, 1993.
- Saxena, S. K., G. Shen, and P. Lazor, Temperatures in Earth's core based on melting and phase transformation experiments on iron, *Science*, **264**, 405-407, 1994.
- Scarfe, C. M., and E. Takahashi, Melting of garnet peridotite to 13 GPa and early history of the upper mantle, *Nature*, **322**, 354-356, 1986.
- Schmitt, D. R., and T. J. Ahrens, Shock temperatures in silica glass: Implications for modes of shock induced deformation, phase transformation, and melting with pressure, *J. Geophys. Res.*, **94**, 5851-5871, 1989.
- Serghiou, G., A. Zerr, L. Chudinovskikh, and R. Boehler, The coesite-stishovite transition in a laser-heated diamond cell, *Geophys. Res. Lett.*, **22**, 441-444, 1995.
- Shankland, T. J., and J. M. Brown, Homogeneity and temperatures in the lower mantle, *Phys. Earth Planet. Inter.*, **38**, 51-58, 1985.
- Shen, G., P. Lazor, and S. K. Saxena, Melting of wüstite and iron up to pressures of 600 kbar, *Phys. Chem. Mineral.*, **20**, 91-96, 1993.
- Sweeney, J. S., and D. L. Heinz, Melting of iron-magnesium-silicate perovskite, *Geophys. Res. Lett.*, **20**, 855-858, 1993.
- Tamai, H., and T. Yagi, High pressure and high temperature phase relations in CaSiO_3 and $\text{CaMgSi}_2\text{O}_6$ and elasticity of perovskite-type CaSiO_3 , *Phys. Earth Planet. Inter.*, **54**, 370-377, 1988.
- Weertman, J., and J. R. Weertman, High temperature creep of rock and mantle viscosity, *Annu. Rev. Earth Planet. Sci.*, **3**, 293-315, 1975.
- Weng, K. H. K. Mao, and P. M. Bell, Lattice parameters of the perovskite phase in the system MgSiO_3 - CaSiO_3 - Al_2O_3 , *Year Book Carnegie Inst. Wash.*, **81**, 273-277, 1982.
- White, W. B., Structural interpretations of lunar and terrestrial minerals by Raman spectroscopy, in *Infrared and Raman Spectroscopy of Lunar and Terrestrial Materials*, edited by C. Karr, pp. 325-358, Academic, San Diego, Calif., 1975.
- Williams, D. W., and G. C. Kennedy, Melting curve of diopside to 50 kilobars, *J. Geophys. Res.*, **74**, 4359-66, 1969.

- Williams, Q., and R. Jeanloz, The high pressure melting curve of iron: A technical discussion, *J. Geophys. Res.*, **96**, 2171-2184, 1991.
- Yagi, T., and S. Akimoto, Direct determination of coesite-stishovite transition by in situ X-ray measurements, *Tectonophysics*, **35**, 259-270, 1976.
- Yagi, T., and J. Susaki, A laser heating system for diamond anvil using CO₂ laser, in *High-Pressure Research: Application to Earth and Planetary Sciences*, *Geophys. Monogr. Ser.*, vol. 67, edited by Y. Syono and M. H. Manghnani, pp. 51-54, AGU, Washington, D. C., 1992.
- Zerr, A., and R. Boehler, Melting of (Mg,Fe)SiO₃-perovskite to 625 kilobars: Indication of a high melting temperature in the lower mantle, *Science*, **262**, 553-555, 1993.
- Zhang, J., and C. Herzberg, Melting of pyrope, Mg₃Al₂Si₃O₁₂, at 7-16 GPa, *Am. Mineral.*, **79**, 497-503, 1994.
- Zhang, J., R. C. Liebermann, T. Gasparik, C. T. Herzberg, and Y. Fei, Melting and subsolidus relations of SiO₂ at 9-14 GPa, *J. Geophys. Res.*, **98**, 19,785-19,793, 1993.

P. Lazor and G. Shen, Geophysical Laboratory, Carnegie Institution of Washington, 5251 Broad Branch Road, N.W., Washington, DC 20015.

(Received September 2, 1994; revised May 30, 1995; accepted June 6, 1995.)